Accepted submission to the ASME 2024
Pressure Vessels & Piping Conference

STRAIN-RATE-DEPENDENT PARAMETERS OF LITHIUM AS A PLASMA FACING MATERIAL FOR MAGNETIZED TARGET FUSION APPLICATION

Yu Miao[1,*], Michael Sexsmith[1], Soegi Hartono[1], Claire Preston[1], Benjamin Tsai[1], Jean-Sebastien Dick[1], Nick Sirmas[1]

[1]General Fusion, Richmond, British Columbia, Canada

ABSTRACT

Lithium is an ideal plasma facing material for fusion plasmas due to its low atomic mass, ability to breed tritium fuel and its gettering characteristics. Liners made of lithium are used as magnetic flux conservers, which can be compressed for Magnetized Target Fusion (MTF) applications. Lithium has been extensively examined in the literature aiming at its mechanical properties for its various applications, and yet the knowledge about its mechanical properties is insufficient for the MTF application in two aspects. First, most of the available studies focus on the quasi-static loading cases. Second, the tests in those studies were commonly performed via uniaxial tensile test where the stress state was not representative for the compression loading scenario.

In this paper, we present an approach to estimate parameters that govern lithium's behavior at high strain rates up to 500 s^{-1}. In our approach, a series of drop-piston experiments were combined with ANSYS LS-DYNA simulation to determine the material parameters. The bi-linear strain hardening model and Johnson-Cook material model were considered in our studies where the former one accounts for the plastic stress-strain relationship and the latter one describes the plastic stress-strain relationship with the strain-rate effects. In our drop-piston experiments, we use high-speed camera imaging and a feature tracking algorithm to record the velocity and extract the piston impact time. A bi-linear strain hardening model was initially used to estimate plastic behavior of lithium. The strain-rate dependent material parameters were then determined using a reverse engineering approach with the help of numerical simulations that reproduce the tests. A series of numerical simulations with different combinations of material parameters were computed to establish the combination of material parameters that best fit the test results.

The proposed material model will be used in the lithium compression experiments for MTF applications, which accounts for the hardening behavior at different strain rates.

Keywords: Lithium, strain rate dependent, impact test, ANSYS LS-DYNA, Magnetized Target Fusion (MTF)

*Corresponding author: paul.miao@generalfusion.com

NOMENCLATURE

ε	strain
ε_p	plastic strain
$\dot{\varepsilon}$	dimensionless strain rate
$\dot{\varepsilon}_0$	reference strain rate
σ	stress
σ_y	yield stress
A	specimen cross-sectional area
B	strain hardening constant
C	strain rate hardening coefficient
E	modulus of elasticity
K	hardening parameter
k	linear strain hardening
L	specimen length
m	thermal softening exponent
M	piston mass
n	hardening coefficient
T^*	homologous temperature

1. INTRODUCTION

The low atomic weight, softness, and high ductility of lithium make understanding the mechanical behavior of the material of engineering significance. When utilized as a liner, lithium's exceptional compressibility makes it an ideal material for serving as a magnetic flux conserver in the context of Magnetized Target Fusion (MTF) [1, 2].

In recent years, the mechanical behavior of lithium has been widely investigated through various testing methods, including indentation [3, 4], tension [5, 6], and bending [7, 8], within the fields of automotive and battery industries; but there is a limited number of studies related to the mechanical parameters of lithium under compressive impaction. It is known that quasi-static loading, from a mechanics viewpoint, does not have a significant influence on the yield stress of lithium, nor the corresponding stress-strain relationship. The increased values of the strain rate cause an increase in the yield stress of lithium and large inelastic deformations can develop, typically, at high rates of deformation from impaction [9, 10].

The purpose of this study is to bridge the gap in studies of the mechanical parameters of lithium by 1) performing large-

deflection impact tests on the lithium samples under uniaxial stress states, and 2) by characterizing the measured mechanical behavior under high rates of strain. These goals are accomplished using a series of drop impact tests.

Simulations of the drop test are performed using Finite Element (FE) analysis to determine the strain-rate dependency of the material's plastic curve. A series of numerical simulations with different combinations of material parameters are carried out to establish the best combination of parameters that fit the results of the physical experiment. Central Composite Design (CCD) is employed to expedite the computation time required for estimating material parameters, given that the strain-rate-dependent parameters can cover a range spanning many orders of magnitude. The calculated parameters of lithium will be compared with tests previously published in the literature.

2. EXPERIMENTAL SETUP

2.1 Piston Drop Test Bed

The test consisted of a jig that was made of a vertical aluminum tube with an inner diameter of 38 mm. The jig was then mounted directly above a SAE 304 stainless anvil base, as shown in Fig. 1. The anvil base had a diameter of 152 mm, and a height of 450 mm. The tube was attached to a gimbal to ensure that it was vertical, and the anvil was levelled such that its face was perpendicular to the axis of the tube. Several lateral holes were made in the tube at different altitudes to determine the various drop heights. A high-speed camera was set up with its center of view at 10 mm above the anvil surface.

For each test, the piston was positioned at its initial height and a trigger pin was used to hold it in position. A lithium sample was centered under the tube with a plexiglass guard placed around the sample. The trajectory of the piston was initiated by the removal of the pin. At 300 mm above the sample another pin is triggered by the falling piston to initiate the video capture. The displacement of the anvil is not recorded during the test due to its significantly higher mass, which is orders of magnitude greater than that of the piston. The piston velocity relative to the frame of the camera was an accurate representation of the piston deceleration. Due to the low mass of the sample, the transferred kinematic energy to the sample was negligible. Consequently, the deceleration of the piston was primarily attributed to the deformation of the sample.

A series of drop impact tests was conducted using pistons of different lengths, resulting in varying weights. The pistons were also dropped from varying heights to obtain a range of kinetic energies, as summarized in Table 1.

To achieve both high strain rates and large plastic strains, the piston weight and the drop height were chosen such that the shape of the deformed sample was less than a height of 15 mm, which is approximately equivalent to 30-50% of the total strain, as shown in Fig. 2.

All samples were coated in mineral oil prior to the drop test to prevent friction from impacting the test results. The friction impeding the radial expansion of the sample, in contact with both the anvil and the piston surfaces, was deemed negligible in comparison to the radial growth induced by the deformation. The severe barreling effect was not observed in the deformed samples.

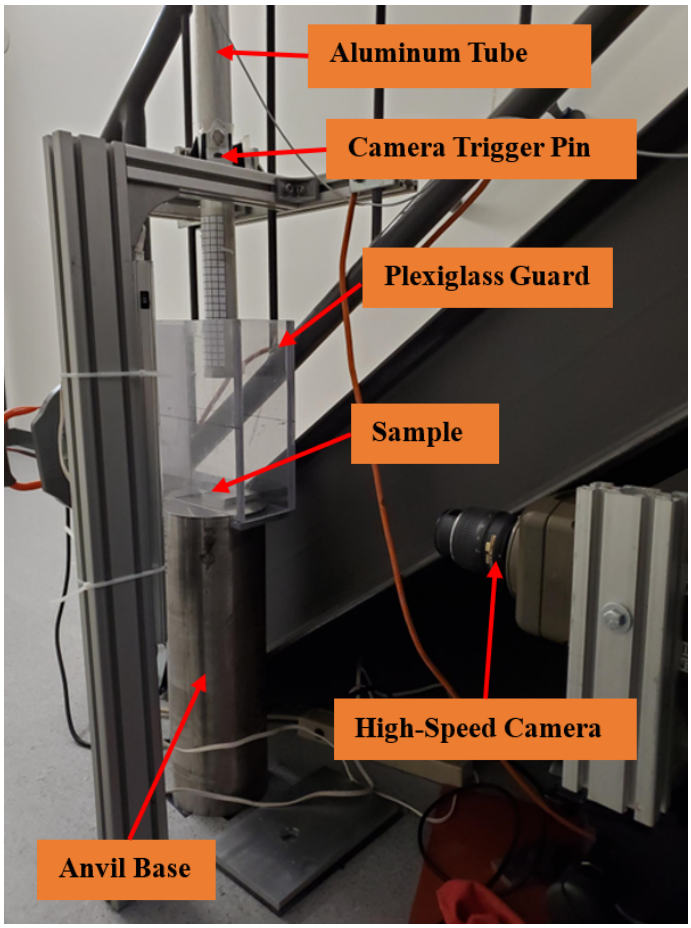

FIGURE 1: Experimental setup for the drop-test

To ensure result accuracy, the drop test was repeated three to five times for each test case.

2.2 Lithium Sample Preparation

Lithium samples were sourced from recycled lithium due to limited supply. The purity of the lithium samples was not evaluated; however, oxidation layers were thoroughly removed. All lithium samples shared consistent dimensions: 22 mm in height and 18 mm in diameter.

The lithium samples were prepared using an SAE 304 stainless-steel mold equipped with a cartridge heater positioned at the mold's base to maintain a constant temperature of 50°C, as illustrated in Fig. 3. Sample preparation was executed in an argon atmosphere. When the sample reached 250°C, which is higher

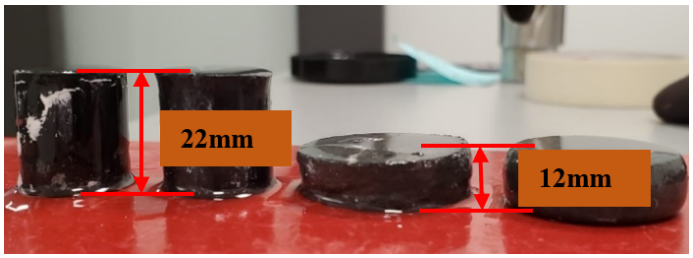

FIGURE 2: Comparison between initial and deformed samples

TABLE 1: Summary of test conditions for the different cases investigated

Test Case	Piston Weight (g)	Drop Height (mm)	Impact Energy (J)	Deformed Height (mm)	Deformed Diameter (mm)	Total Strain (%)
A	882	5280	45.07	13-13.9	23-23.5	38-39
B	882	3810	32.95	15.3-15.7	21.9-22.6	30-31
C	1325	5280	68.59	10.5-11	25.5-26	50-51

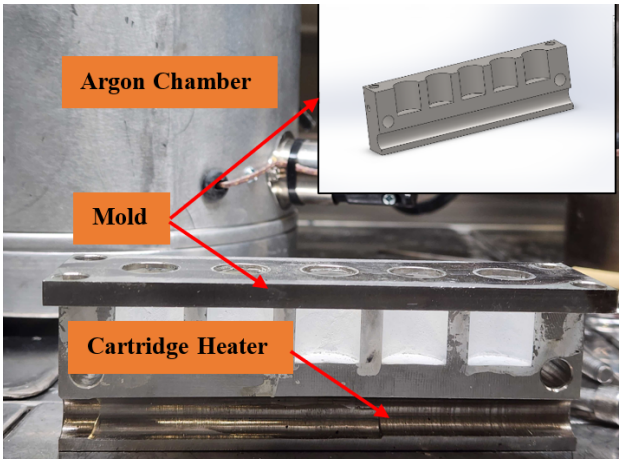

FIGURE 3: SAE 304 stainless-steel mold in argon chamber

than the melting point of lithium (150°C), the lithium sample was poured into the mold. The lithium sample could be easily removed from the mold because of the different degrees of thermal conductivity of lithium versus that of 304 stainless-steel. After being removed from the mold the samples were coated in mineral oil to prevent oxidation.

2.3 Data Collection and Post-Processing

A computer vision based scientific program was developed in Python© to track the position of the piston near the moment of impact. The program uses gradients of the pixel map to detect the edges of the piston and the width of the lithium sample (Fig. 4a). The width of the piston is used as a reference to convert pixels to distance measurements.

The velocity of the piston was calculated using finite differences. The impact between the sample and piston was determined to start when the pellet width starts to grow. A linear fit using the sample width data after impact was used to re-assess the time of impact, since it is critical for calculating the strain rate. Smoothing algorithms were then used to remove noise from the video measurements. A visualization of this process is shown in Fig. 4b.

The flow stress from the test data was calculated based on the force estimated using less than 10 discrete data points per test. To reduce noise in the displacement data, the velocity was computed by considering the total displacement over 20 time steps divided by the overall time for these 20 data points. The acceleration was then derived using a similar approach. This approach helps ensure a more accurate estimation of the flow stress from the experimental data.

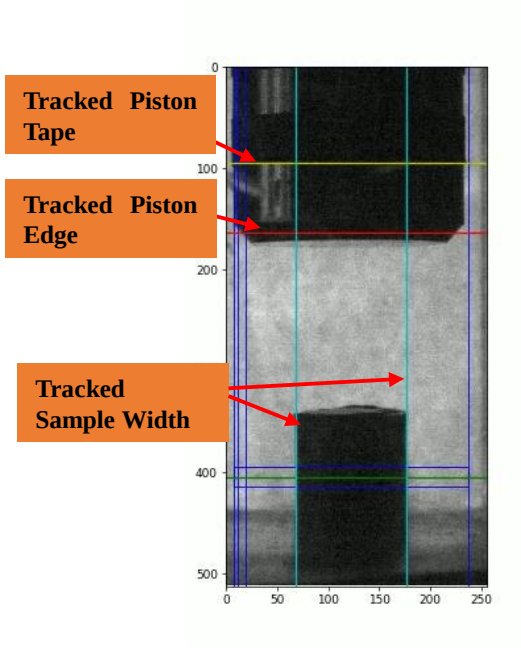

(a)

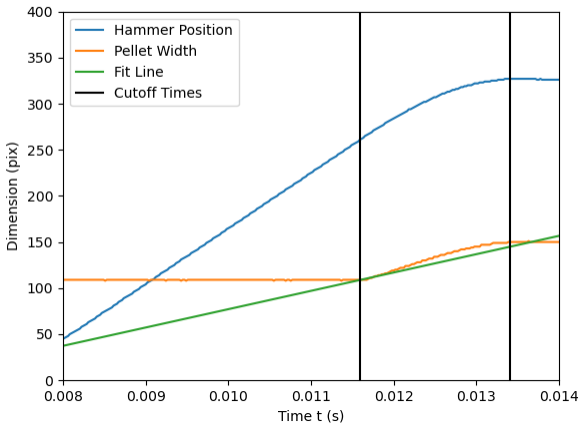

(b)

FIGURE 4: Tracking algorithm results: (a) Video frame with overlay of tracked piston and sample width, (b) Plot of hammer position and sample width over time, indicating cutoff times for strain data analysis.

TABLE 2: Mesh statistics for axi-symmetric LS-DYNA simulations

	Total Number of	
Test Case	Elements	Nodes
A and B	1889	1986
C	2837	2985

3. NUMERICAL MODELS

3.1 Material Model

Two material models were derived to represent the compression behavior of lithium: the bi-linear hardening model and the Johnson-Cook model.

3.1.1 Bi-Linear Hardening Model. The bi-linear hardening model, which does not incorporate an explicit term for the strain rate in its formulation, is determined based on the following parameters: yield stress (σ_y), linear strain hardening constant (K) and plastic strain (ε_p). This material model is the simplest description of a complex plastic behaviour, and its flow stress is expressed as:

$$\sigma = \sigma_y + K\varepsilon_p \tag{1}$$

3.1.2 Johnson-Cook Material Model. The Johnson-Cook material model [11] incorporates strain-rate dependent characteristics and thermal softening. The Johnson-Cook material model uses the following material constants: σ_y, B, n, C, and m. These constants are defined as follows: σ_y is the yield stress of the material under reference conditions, B is the strain hardening constant, n is the strain hardening coefficient, C is the strengthening coefficient of strain rate, and m is the thermal softening coefficient.The flow stress is then given by:

$$\sigma = \left[\sigma_y + B\left(\varepsilon_p\right)^n\right]\left[1 + C\ln\left(\frac{\dot{\varepsilon}}{\dot{\varepsilon}_0}\right)\right]\left[1 - T^{*m}\right] \tag{2}$$

where $\dot{\varepsilon}$ is the strain rate, $\dot{\varepsilon}_0$ is the reference strain rate, and T^* is the homologous temperature ($T^* = (T - T_{ref})/(T_{melt} - T_{ref})$). In the present study, the melting temperature of lithium is assumed to be $T_{melt} = 180°C$, and reference temperature is set to $T_{ref} = 21°C$.

Equation (2) measures how the strain rate influences the flow stress σ. The flow-stress curves are not linear, and the non-linearity depends on the exponent n. As the strain rate increases, the flow-stress curve also experiences an increase.

3.2 Ansys LS-DYNA Model

3.2.1 FE Model Setup. The explicit solver in LS-DYNA was used to determine the material parameters of the Johnson-Cook model. A 2D axi-symmetric FEA model was established to simulate the drop impact on the lithium sample, as shown in Fig. 5. The geometry was discretized using first-order hexagonal elements, with a finer mesh specifically applied to the contact area to ensure accurate representation of contact at impact. The resulting mesh statistics are listed in Table 2.

The anvil base was vertically restrained at the bottom face, adequately securing the model, and preventing rigid body motion.

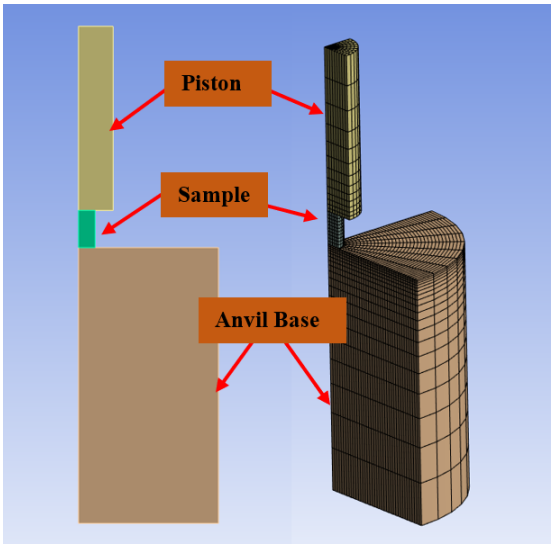

FIGURE 5: Axi-symmetric FE model used in LS-DYNA

The initial state was established by applying general gravity, allowing the sample to settle on the base. Subsequently, the impact velocity was applied to the piston to replicate the actual impact conditions. The contact between all parts utilized a symmetrical frictional contact between fitting surfaces with the friction coefficient of 0.1.

The elastic-plastic material model for the piston, made from SAE 304 stainless steel, was constructed using the Ramsberg-Osgood equation. The elastic material model with Young's modulus of 195 GPa was assigned to the anvil base, which is significantly more rigid compared to the lithium sample.

3.2.2 Design Optimization. The Johnson-Cook parameters were determined through design optimization, aiming to achieve a correspondence between the numerical calculation of the piston displacement and the experimental position of the piston. A considerable number of optimization calculations were performed to achieve an appropriate fitting. The optimization iteration procedure is summarized as follows:

1. In total 5 parameters (outlined in Tables 3 and 4) were determined. Different combinations of these parameters were carried out to best fit the experimental results. By using CCD, the assigned combinations of parameters are approximately equally distributed over the search space, thus resulting in a significant reduction in the number of studies required [12].

2. A response surface was constructed based on the assigned combinations to provide the approximated values of the output parameters without the need to perform a complete solution. Full second order polynomials were used to fit the response surface and the verification points were also applied to assess its quality. The verification points compare the predicted and observed values of the output parameters at different locations of the design space.

3. Optimization was performed based on the established response surface. An iterative genetic algorithm associated

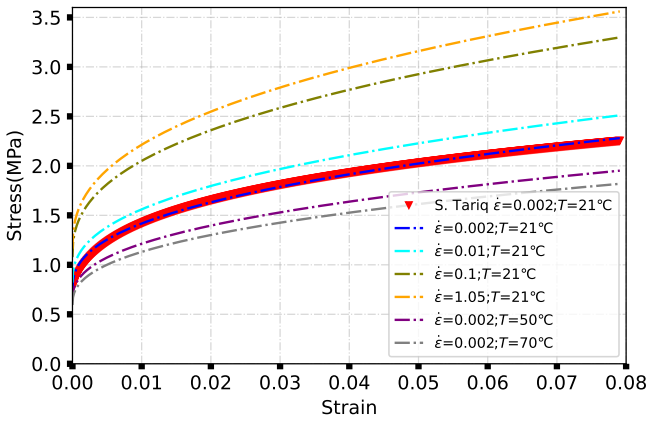

FIGURE 6: Comparison of the estimated Johnson-Cook Model with the experimental strain hardening curves conducted by S. Tariq [7]

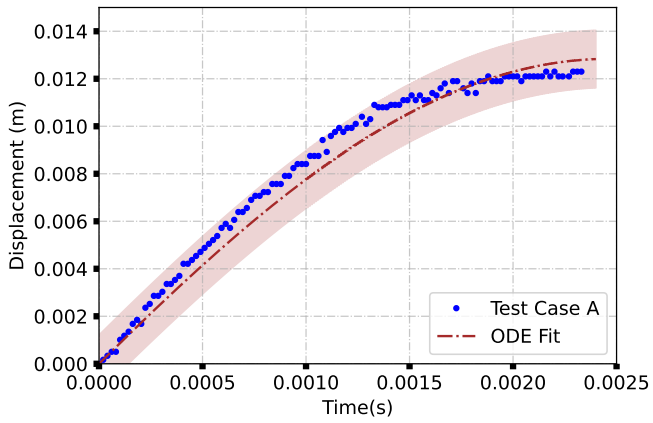

FIGURE 7: ODE best fit to drop test A, with maximum fitting errors at 17%

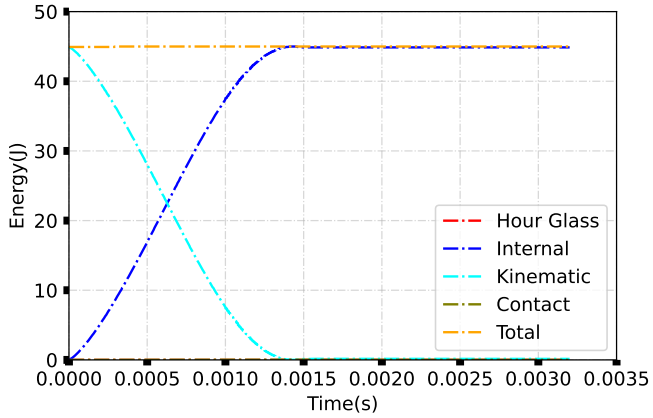

FIGURE 8: The evolution of energies extracted from the simulation of drop test A

with a cost function that measured the deviations of the experimental and simulation results was used for the optimizations. This algorithm was a more refined approach as it iteratively narrowed the differences between the experimentally determined data and the simulated data until the best fit was determined.

4. RESULTS AND DISCUSSION

4.1 Johnson-Cook Material Model from Literature

In this study, the initial Johnson-Cook material model parameters were estimated based on the strain rate dependence tests done by S. Tariq [7]. The modulus of elasticity (E) and hardening parameters (K and n) were extracted from tests conducted at various strain rates and temperatures, as detailed in Table 1 of Ref. [7]. The strain hardening curves were reconstructed by using plastic strain-hardening from Eq. (3) with the parameters outlined in Ref. [7].

$$\sigma = K\varepsilon_{\mathrm{p}}^{n} \tag{3}$$

The strain hardening parameters σ_{y}, B, and n in Eq. (2) were determined by fitting to the reconstructed strain hardening curves. Linear interpolation was used to determine the strain rate parameters C and thermal softening parameter m in Eq. (2). The resulting strain hardening curves based on the Johnson-Cook model were then matched to their experimental counterparts as illustrated in Fig. 6. The estimated model parameters by Ref. [7] are summarized in Table 4.

4.2 Bi-Linear Strain Hardening Fitting

The system of ordinary differential equations (ODEs) (4) and (5) were developed from Eq. (1) and expressed as:

$$M \times \left(1 + \frac{K}{E}\right) \times \dot{v} = -\sigma_{\mathrm{y}} + \left(\left(\frac{K \times x}{L}\right) \times A\right) \tag{4}$$

$$\dot{x} = v \tag{5}$$

where A is the cross-section area, L is the length of lithium sample, and M is weight of the piston.

By solving the ODEs (4) and (5), the solution that provides the best fit for the piston positions in drop test A is shown in Fig. 7, resulting in a hardening constant K, yield stress σ_{y}, and Young's modulus E of 33.6 MPa, 1.1 MPa and 8.35 GPa, respectively.

4.3 Numerical Results

4.3.1 Initial Results. Figure 8 illustrates the variation in impact energy over time during the impact period for drop test A, where an impact velocity of 10.11 m/s was recorded. Consistent with the experimental kinematic energy outlined in Table 1, the simulation demonstrates an initial kinetic energy of 44.97 J, with this energy decreasing as it converts to internal (strain) energy within the lithium sample.

Figure 9 shows the simulation results of the displacement of the piston using the Johnson-Cook parameters from [7], against the experimental measurements. Additionally, Fig. 9 shows the calculated strain rate is approximately 600 s^{-1} at the time of impact near 0.001 s. The strain rate decreases rapidly to a quasi-static rate over the following 0.001 s. The simulated piston displacement matches the experimental data up to the time of impact. A divergence between the simulated and experimental

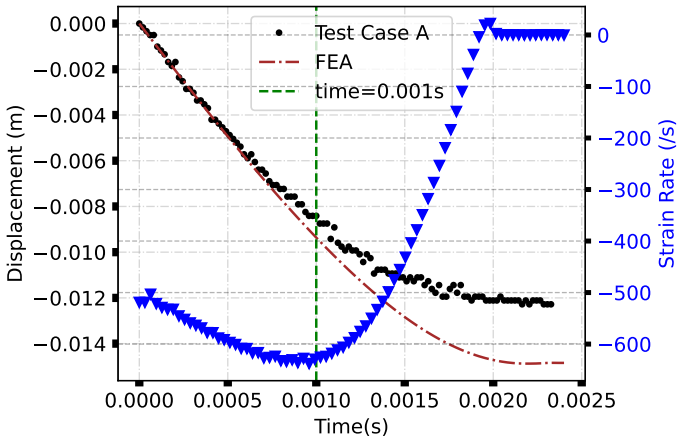

FIGURE 9: Comparison of piston displacement obtained from test and simulation for drop test A. Also shown is the instantaneous strain rate estimated from the test.

TABLE 3: Design point range

Design Range	Hardening Constant, B (MPa)	Strain Rate Constant, C	Hardening Exponent, n	Young's Modulus, E (GPa)	Initial Yield Stress, σ_y (MPa)
Lower	10.0	0.010	0.30	7.48	0.684
Mean	15.0	0.020	0.60	8.74	0.842
Upper	20.0	0.035	0.90	10.0	1.00

piston displacement becomes apparent following the time of impact, coinciding with the decrease in strain rate. This deviation suggests that a higher strain rate constant and a lower hardening constant were used in this Johnson-Cook model. This aligns with the bi-linear strain hardening fitting results detailed in Sec. 4.2, where the calculated strain hardening is 33.7 MPa compared to 1.1 MPa.

4.3.2 Optimized Results. Table 3 shows factor levels for the original domains of the Johnson-Cook parameters with the application of CCD. In total 27 combinations were executed, comprising 17 design points and 10 verification points. The five Johnson-Cook parameters chosen for the design optimization were σ_y, B, n, C, and E, with the domain of each parameter selected based on the initial fitting.

By using full second order polynomials, the numerical response surface provided an accurate relationship between Johnson-Cook parameters and piston position at each stage of the impact tests, ranging from 0.0005-0.0015 s, as illustrated in Fig. 10.

The optimized Johnson-Cook parameters are summarized in Table 4. Figure 11 shows that the numerical piston displacement corresponds well with the test data, indicating a successful optimization of the Johnson-Cook model.

From Table 4, it is evident that the optimized Johnson-Cook parameters exhibit a higher strain hardening constant, but a lower strain rate constant compared to the parameters fit from literature, consistent with the initial findings. Furthermore, in comparison

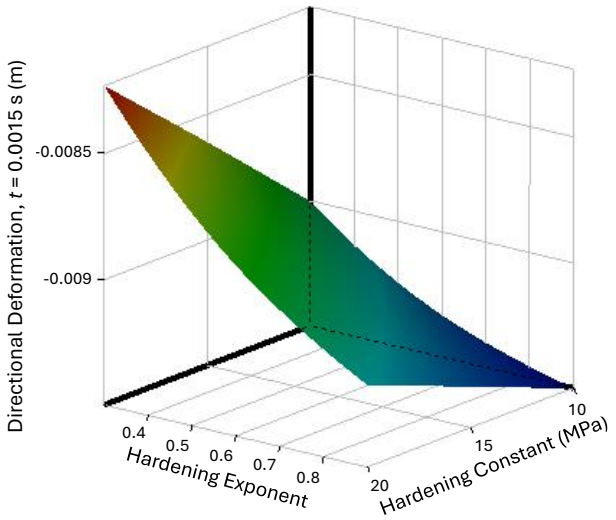

FIGURE 10: An example of a 3D response surface: correlation of hardening exponent and constant against piston position

TABLE 4: Summary of material characteristics

	Literature Fit [7]	Bi-Linear Strain Hardening Fit	Optimized Fit
Young's Modulus, E (GPa)	7.80	8.35	7.82
Initial Yield, σ_y (MPa)	0.760	1.1	0.744
Hardening Constant, B (MPa)	4.19	33.6	19.8
Hardening Exponent, n	0.40	N/A	0.30
Strain Rate Constant, C	0.049	N/A	0.0141
Thermal Softening Exponent, m	0.77	N/A	0.77

to the bi-linear strain hardening fitting, the optimized parameters have a lower hardening constant, although both fittings demonstrate values for E and σ_y that are close. Our interpretation is that this discrepancy arises from the absence of consideration for the strain rate constant in the bi-linear strain hardening fitting. When solving the ODE to match the experimental data, the observed strain hardening attributed to the high strain rate contributes to a higher hardening constant.

In Fig. 12, the directly calculated flow stress from the test data aligns well with the flow stress predicted by the Johnson-Cook model using the optimized parameters.

5. CONCLUSION

A series of hammer drop tests using a piston were conducted to assess the strain rate and plastic strain hardening of lithium. A computer program was developed to monitor the vertical position and velocity of the piston, utilizing time-lapse videos recorded by a high-speed camera. This information was adequate for calculating both the strain and strain rate of the lithium sample under compressive loading.

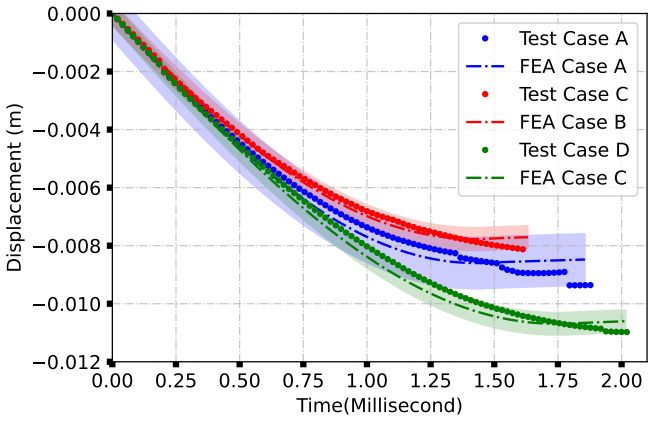

FIGURE 11: Comparison of the piston positions over time obtained experimentally and numerically (using the optimized Johnson-Cook fit), resulting in maximum fitting errors of 10% (Case A), 5.1% (Case B), and 4.3% (Case C)

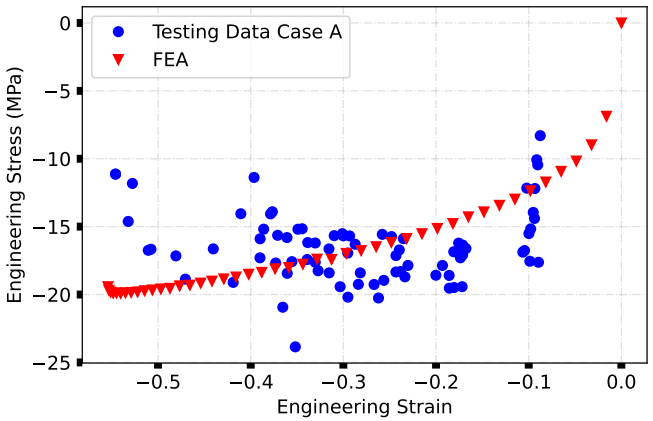

FIGURE 12: Flow stress estimated from the Johnson-Cook function and test data for case A (Root Mean Square Error=5.3)

Both the bi-linear strain hardening model and the Johnson-Cook material model were chosen to characterize the plastic stress-strain relationship of the lithium sample under variable strain rates. The coefficients of the bi-linear strain hardening model were determined through residual minimization, involving the difference between the predicted position of the piston, as per the equation of motion, and the actual trajectory measurements.

The LS-DYNA explicit solver was employed to ascertain the material parameters of the Johnson-Cook model. These parameters were obtained by the minimization of a cost function using a genetic algorithm. A comparison between experiments and simulations reveals a consistent agreement between the optimized Johnson-Cook model predictions and the outcomes of the drop tests. It is noteworthy that the optimized Johnson-Cook parameters exhibit a lower hardening constant than the fitting obtained from the bi-linear strain hardening model. This discrepancy can be attributed to the exclusion of the strain rate constant in the bi-linear strain hardening fitting. Both material models can be used in numerical solvers to carry simulations involving plastically deforming lithium.

ACKNOWLEDGMENTS

We would like to express our sincere gratitude to SimuTech Group for their invaluable assistance in the simulation aspects of this work. Their expertise and support played a crucial role in enhancing the quality and depth of our research.

REFERENCES

[1] Laberge, M. "Magnetized target fusion with a spherical tokamak." *Journal of Fusion Energy* Vol. 38 No. 1 (2019): pp. 199–203.

[2] Ono, M. "Lithium as plasma facing component for magnetic fusion research." Technical Report No. PPPL-4808. Princeton Plasma Physics Lab.(PPPL), Princeton, NJ (United States). 2012.

[3] Yamanaka, T., Takagishi, Y., Tozuka, Y. and Yamaue, T. "Modeling lithium ion battery nail penetration tests and quantitative evaluation of the degree of combustion risk." *Journal of Power Sources* Vol. 416 (2019): pp. 132–140.

[4] Chung, S. H., Tancogne-Dejean, T., Zhu, J., Luo, H. and Wierzbicki, T. "Failure in lithium-ion batteries under transverse indentation loading." *Journal of Power Sources* Vol. 389 (2018): pp. 148–159.

[5] Liu, B., Zhang, J., Zhang, C. and Xu, J. "Mechanical integrity of 18650 lithium-ion battery module: Packing density and packing mode." *Engineering Failure Analysis* Vol. 91 (2018): pp. 315–326.

[6] Sheikh, M., Elmarakbi, A. and Elkady, M. "Thermal runaway detection of cylindrical 18650 lithium-ion battery under quasi-static loading conditions." *Journal of Power Sources* Vol. 370 (2017): pp. 61–70.

[7] Tariq, S., Ammigan, K., Hurh, P., Schultz, R., Liu, P. and Shang, J. "Li material testing-fermilab antiproton source lithium collection lens." *Proceedings of the 2003 Particle Accelerator Conference*, Vol. 3: pp. 1452–1454. 2003. IEEE.

[8] Tang, C., Yuan, Z., Liu, G., Jiang, S. and Hao, W. "Acoustic emission analysis of 18,650 lithium-ion battery under bending based on factor analysis and the fuzzy clustering method." *Engineering Failure Analysis* Vol. 117 (2020): p. 104800.

[9] Xu, J., Jia, Y., Liu, B., Zhao, H., Yu, H., Li, J. and Yin, S. "Coupling effect of state-of-health and state-of-charge on the mechanical integrity of lithium-ion batteries." *Experimental Mechanics* Vol. 58 (2018): pp. 633–643.

[10] Xi, S., Zhao, Q., Chang, L., Huang, X. and Cai, Z. "The dynamic failure mechanism of a lithium-ion battery at different impact velocity." *Engineering Failure Analysis* Vol. 116 (2020): p. 104747.

[11] Škrlec, A. and Klemenc, J. "Estimating the strain-rate-dependent parameters of the Cowper-Symonds and Johnson-Cook material models using Taguchi Arrays." *Strojniški vestnik-Journal of Mechanical Engineering* Vol. 62 No. 4 (2016): pp. 220–230.

[12] Lee, K.., Park, S. and Han, T. "Finite element analysis of the drop test for plastics using tensile properties at high strain rates." *2007 International Forum on Strategic Technology*: pp. 77–80. 2007. IEEE.